S & M 4192

Charging the Battery of an Implanted Cardiac Pacemaker Using Thermoelectric Generator Modules

Shang-Kuo Yang, Bei-Fu Ou, Kai-Jung Chen, and Wei-Shen Kuo*

Department of Mechanical Engineering, National Chin Yi University of Technology, Taichung 41170, Taiwan, R.O.C.

(Received May 22, 2025; accepted October 1, 2025)

Keywords: thermoelectric, cardiac pacemaker, charging

In this study, our purpose is to recharge the battery of an implanted pacemaker using the electrical energy generated by thermoelectric modules. As long as a temperature gradient is applied, it can drive the thermoelectric modules to generate electrical energy. The temperature of the human body is almost constant and will not change considerably. Therefore, there is a natural temperature gradient between the human body and the external environment, which can be used to charge the battery of an implanted pacemaker. This approach can resolve effectively the issue of pacemaker failure resulting from power shortage. In this research, we substitute human skin with pig skin to simulate the temperature gradient between the human body and the external environment. The power generation efficiencies of various types and arrangements of thermoelectric modules were experimentally investigated in this work. The results showed that the number of working days of the implantable pacemaker battery is extended differently by different charging durations of the thermoelectric device. Patients undergo only a single implantation surgery, and they do not need to undergo the surgery again for the rest of their life because of power shortage of the battery, thereby reducing patients' risks during surgery, which is thus considerably beneficial to the patients.

1. Introduction

A pacemaker is an implantable device that senses the electrical activity of the heart and regulates the stimulation signals to correct arrhythmia, to maintain a normal rhythm. However, once a pacemaker is implanted in the human body, its power source becomes an issue. A pacemaker's battery typically lasts about 7 to 10 years. When the battery level is low, the patients with implanted pacemakers may experience transient dizziness and other physical discomfort. They will again require surgery to replace the pacemakers. This causes inconvenience and burden to patients, as well as surgical risks. Thus, exploring methods to recharge pacemaker batteries without invasive surgery is important and valuable research. The development of the thermoelectric effect^(1,2) dates back over a century. The thermoelectric effect was discovered in 1821 by the physicist Seebeck. However, limited materials resulted in insignificant progress

*Corresponding author: e-mail: kuows.me88g@nctu.edu.tw
https://doi.org/10.18494/SAM5748

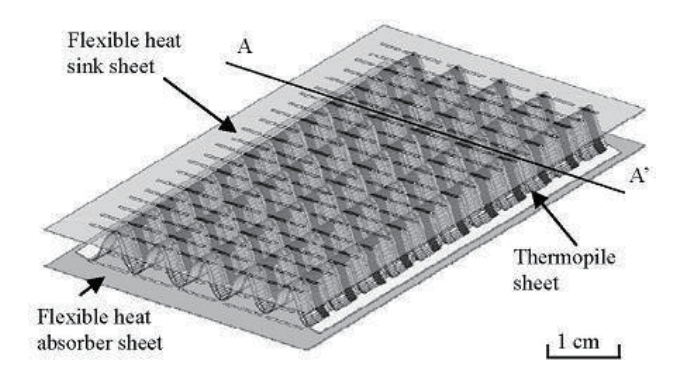
for many years. There was no significant breakthrough in the thermoelectric effect until the rise of semiconductor technology and nanomaterials. For example, the National Aeronautics and Space Administration uses thermoelectric generator model systems as one of the power sources for space exploration satellites. Thermoelectric power generation has gradually become an area of interest in energy generation. Thermoelectric power generation meets environmental requirements, such as low pollution, no noise, long useful life, light weight, and high reliability. It is feasible to generate electricity through a small temperature gradient with current thermoelectric technology. However, issues such as the thermal-to-electrical conversion efficiency of thermoelectric materials and system thermal management need to be resolved.

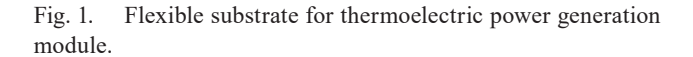
1.1 Literature review

Shiozaki *et al.*⁽⁷⁾ proposed a thermoelectric power generation module using a flexible substrate with p-type and n-type semiconductors deposited on inclined surfaces, as shown in Fig. 1 They applied X-rays to identify the thin film properties of p-type BiTe and achieved a power generation voltage of $160 \, \mu V/K$.

Yu et al.⁽⁸⁾ analyzed the optimal configuration of two-stage thermoelectric modules. In a two-stage thermoelectric module, thermoelectric elements are directly attached to the ceramic surface of the first layer, as shown in Fig. 2. The upper and lower layers of thermoelectric elements can be configured as two independent circuits or connected as a single circuit. The independent circuits for both upper and lower layers were chosen to investigate the effects of the ratio of the number of thermoelectric devices and the length of thermoelectric materials in the upper and lower layers on power generation efficiency.

Daniel *et al.*⁽⁹⁾ utilized the temperature gradient between the human body temperature and the ambient air to generate electricity, applying a thermoelectric generation module to a wristwatch. As shown in Fig. 3, the pillar is the thermoelectric generator module, with heat sinks on the outer surface. The heat of a cold plate dissipates by free convection to maintain the required cold plate temperature for the thermoelectric module. The heat source is provided by the constant heat of the human body, which continuously supplies heat that is higher than the ambient temperature. Owing to the small temperature gradient, the thermoelectric module





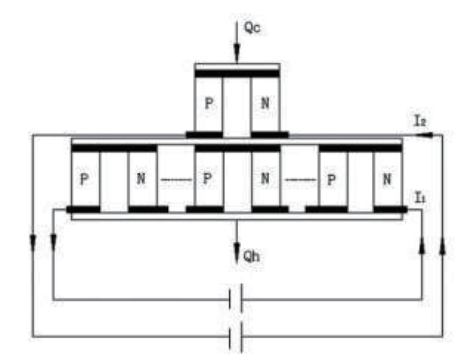


Fig. 2. Two-stage thermoelectric module.

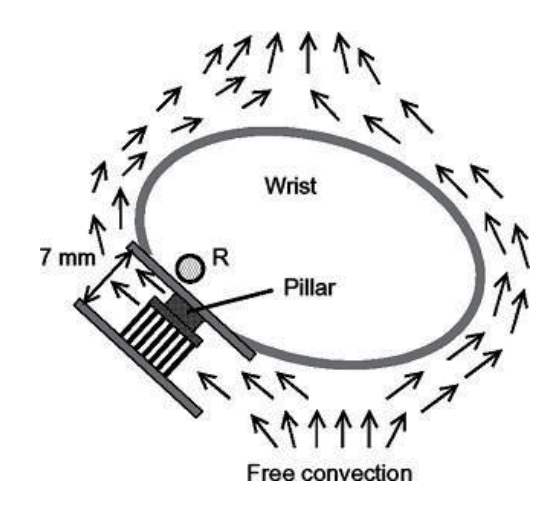


Fig. 3. Schematic of thermopile on wrist.

generates low-power output. However, wristwatches are low-power devices, so the electricity generated by the thermoelectric module is enough to power them. The daily power generation of this thermoelectric module is enough to keep the watch running for several days. Figure 4 shows a prototype of a wrist thermoelectric module.

Rowe and Min⁽¹⁰⁾ fabricated an open porous replica of a polyurethane foam thermoelectric material with an irregular porous network structure, as shown in Fig. 5. The thermoelectric properties and performance of their modules were evaluated. The manufacturing of foams from oxide thermoelectric materials and the concept of using foam structures for waste heat have been discussed, as shown in Fig. 6. The high surface area of the foams allows efficient heat extraction compared with bulk materials.

Rowe and Min⁽¹¹⁾ designed prototype miniature thermoelectric generators that convert heat into electricity owing to the thermopile geometry using P- and N-type semiconductors, as shown in Fig. 7. The conductor/insulator materials alternate their position for each level of the stack to maintain the series connection between the P- and N-type elements, as shown in Fig. 8.

1.2 Research method

The maximum tolerance of the temperature gradient of a human body needs to be determined first, which means determining the lowest ambient temperature that the human body can withstand given a body temperature of 37 °C. The thermoelectric module can generate the maximum electrical energy under the maximum temperature gradient. In this study, the thermoelectric generator module system consists of several thermoelectric modules, and the arrangement and model type can affect the power output of the module. A circuit was designed to solve the unstable voltage and current output of the thermoelectric power generation system. The amount of charge stored in the battery by the thermoelectric charging system can be estimated through discharge experiments. Finally, by comparing the charging amount with the power consumption of an implantable pacemaker, we can determine how long the thermoelectric charging system can extend the continuous operation time of the implantable pacemaker.

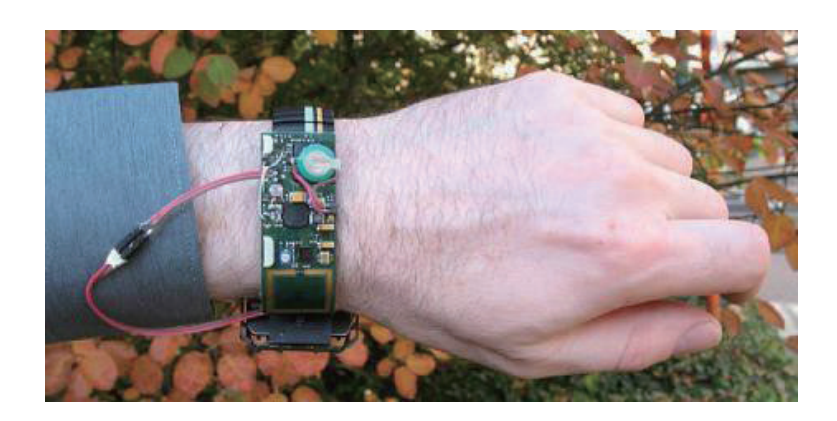


Fig. 4. (Color online) Prototype of bracelet for thermoelectric generation.



Fig. 5. Open porous replica of polyurethane foam.

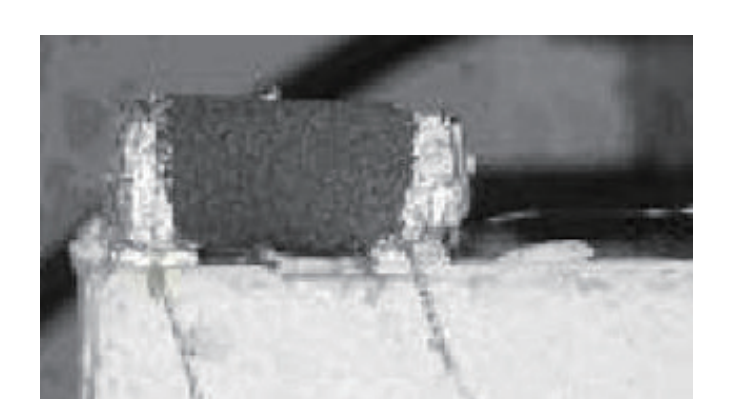


Fig. 6. Thermoelectric foam as thermoelectric generator.

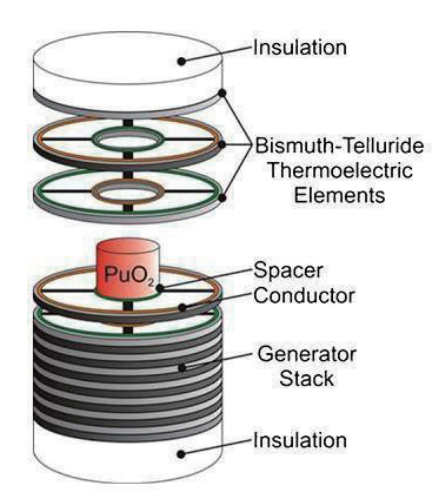


Fig. 7. (Color online) Conceptual design of thermopile.

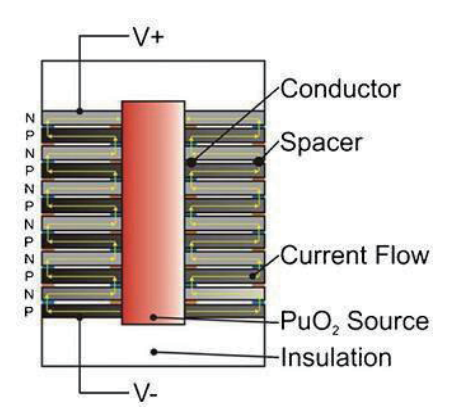


Fig. 8. (Color online) Schematic of heat and current flow.

2. Fundamental Theory

2.1 Pacemaker

2.1.1 Power requirements

There are different types of pacemaker.⁽¹²⁾ In this study, we focus on the pacemaker of the dual-chamber rate-modulated (DDDR) mode; its internal block diagram is shown in Fig. 9.

Table $1^{(13)}$ lists the average current consumption of each unit in the pacemaker, including pacing, sensing amplifier, frequency response sensor, control, and telemetry units. The total average current consumption is $21 \mu A$.

2.1.2 Operating time calculation

Equation (1) is the estimation formula for the operating time of a pacemaker battery. (13)

$$L = \frac{Q}{8766 \times I} \tag{1}$$

Here, L is the estimated operating time of the pacemaker in years, Q is the ampere-hour capacity of the pacemaker battery, 8766 is the total number of hours in a year (365.25 days \times 24 h), and I is the average current consumption of the pacemaker in amperes.

Currently, most pacemaker batteries are lithium batteries with an ampere-hour capacity ranging from about 800 to 3000 mAh. (14) According to Eq. (1), the battery provides enough electricity to keep a pacemaker running continuously for about 7 to 10 years under normal usage. The pacemaker DDDR modes include pacing and sensing (13) with different power consumptions, resulting in various continuous operating times. Table 2(13) shows that the average current consumption without pacing current in the sensing mode is 12 µA. In this study, we assume that an extra battery capacity of 10 mAh of the pacemaker is added by a thermoelectric generator. The operating time in the mode can be extended by about 35 days according to Eq. (1). The average current consumption with pacing current in the pacing mode is 21 µA, as shown in Table 3. (13) With a 10 mAh increase in battery capacity, the operating time in this mode can be extended by about 20 days.

2.2 Thermoelectric generator module

The thermoelectric generator module includes a cold end (heat sink), a hot end (heat source), and a load resistor (RL), as shown in Fig. 10. If a thermocouple has a temperature difference, the thermoelectric effect can be observed as long as each junction does not have the same temperature; this is known as the Seebeck effect.

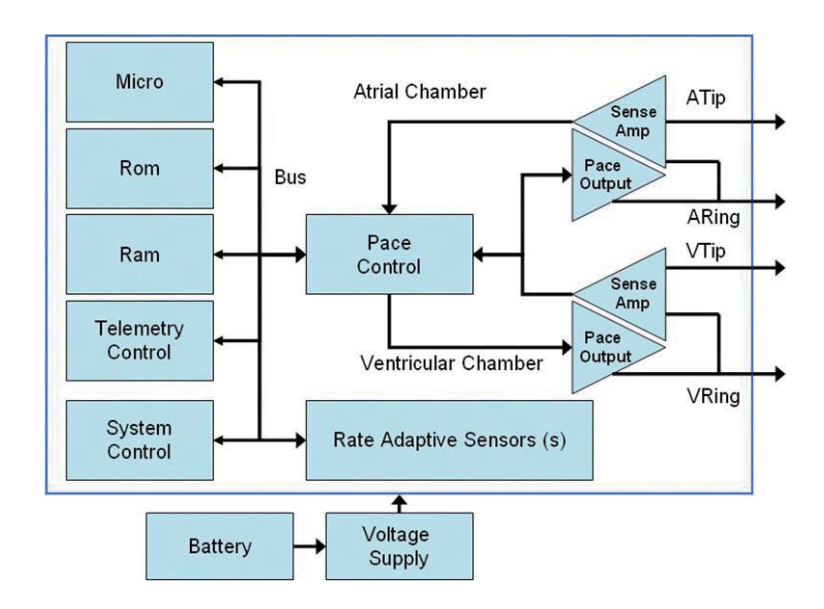


Fig. 9. (Color online) Internal block diagram of DDDR-mode pacemaker.

Table 1 Average current consumption of internal units in pacemaker.

	•		
Function	Peak current drain	Average current drain (µA)	Average current drain as percentage of total (%)
Pacing current	7 mA	8	38
Sense amplifier	2 μΑ	2	10
Rate adaptive sensor	2 μΑ	2	10
Control	16 μΑ	8	38
Telemetry	60 μΑ	<1	4
Total	N/A	21	100

Table 2 Average current consumption of DDDR pacemaker in sensing mode.

\mathcal{C}	1	1	0				
Function		Average current drain (µ					
Sense amplifier			8				
Rate adaptive ser	isor		2				
Control			2				
Total		1	2				

Table 3 Average current consumption of DDDR pacemaker in pacing mode.

Function	Average current drain (µA)
Sense amplifier	8
Pacing Current	8
Rate adaptive sensor	2
Control	2
Telemetry	1
Total	21

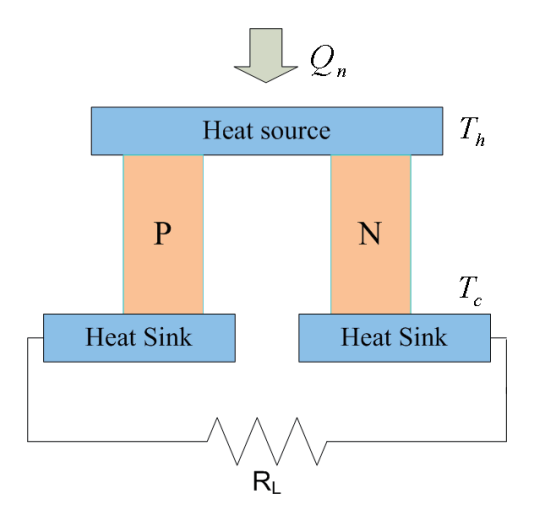


Fig. 10. (Color online) Thermoelectric generator module. Q_n is the input heat power, T_h is the hot-end temperature, T_c is the cold-end temperature, and R_L is the load resistor.

Figure 11 shows equivalent circuit diagram of thermoelectric generator module. According to the Seebeck effect, the voltage (V) generated by the thermoelectric generator module is directly proportional to the temperature difference across its ends if electrons flow from n-type to p-type.⁽¹⁵⁾ The theory to describe this effect is given as

$$V = (S_n - S_p)(T_h - T_c), (2)$$

where S_n is the Seebeck coefficient of the n-type material and S_p is the Seebeck coefficient of the p-type material.

The current generated by the thermoelectric generator module can be calculated as

$$I = \frac{(S_n - S_p)(T_h - T_c)}{R + R_L} \,. \tag{3}$$

3. Experimental Methods and Equipment

3.1 Simulation environment and experimental method

The human body temperature is monitored and regulated by the hypothalamus. When the human body is influenced by external temperatures, the hypothalamus adjusts the body temperature to keep it constant. In this study, thermoelectric modules are placed between the dermal layer (simulated by pig skin) and the subcutaneous fat (simulated by a heat spreader), as shown in Fig. 12. The thermoelectric module generates electricity via the temperature gradient established between the regulated body temperature and the external temperature.

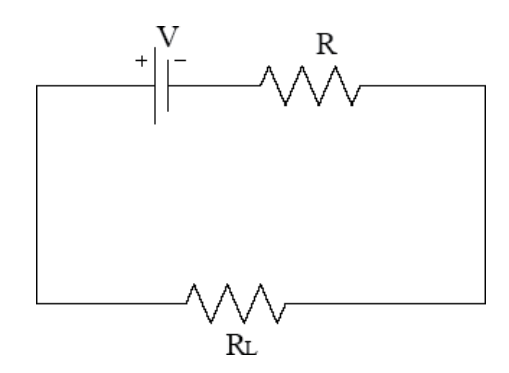


Fig. 11. Equivalent circuit diagram of thermoelectric generator module. V is the voltage generated by the thermoelectric generator module and R is the internal resistance of the thermoelectric generator module.

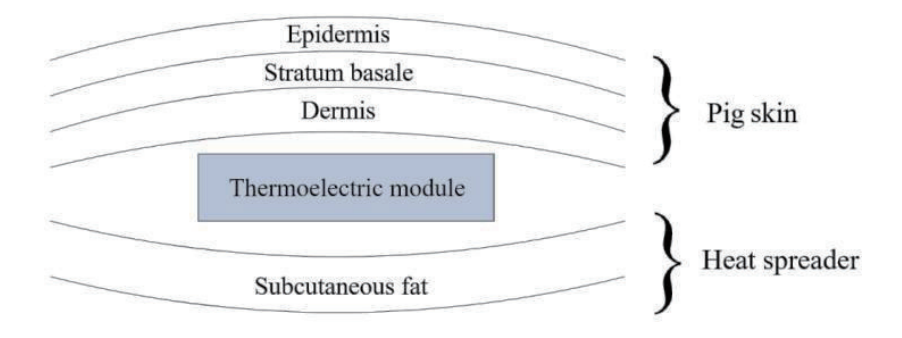


Fig. 12. (Color online) Simulation environment.

3.2 Experimental setup

The power generation efficiency of thermoelectric modules varies with various factors such as their type, the size of semiconductor crystal grains, the length of thermoelectric materials, and various arrangements of thermoelectric modules.

(1) Thermoelectric modules

Five types of thermoelectric module were selected for this study, designated as Samples A, B, C, D, and E, as shown in Fig. 13. The specifications for each sample are described below.

Sample A is manufactured by the German company Micropelt (model number MPG-D602). However, this product was unavailable for purchase. Only the characteristic curve (Fig. 14)⁽¹⁶⁾ provided on the company's website is listed for reference in this study.

Sample B is a thermoelectric cooling module (model number TEC-127.04) with the specifications detailed in Table 4. TEC is the cooling category code (N and P pellet sizes greater than 1 mm), 127 is the number of thermoelectric elements, and 4 A is the maximum operating current

Sample C is a thermoelectric generator module (model number TGM199-1.4-0.8) with the specifications detailed in Table 5. TGM is the generator category code (N and P pellet sizes are

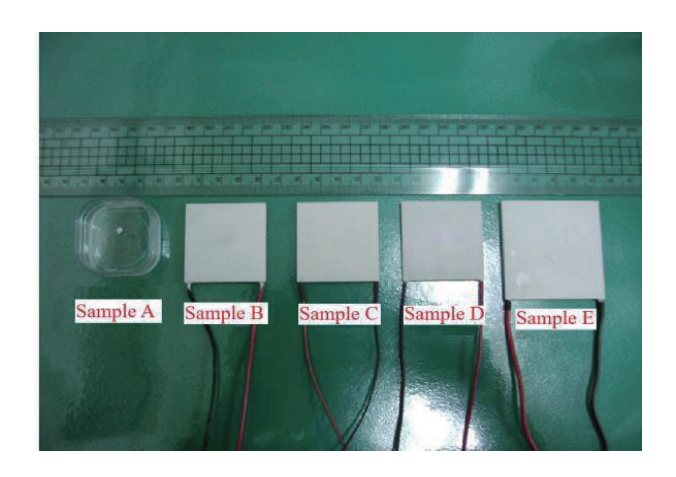
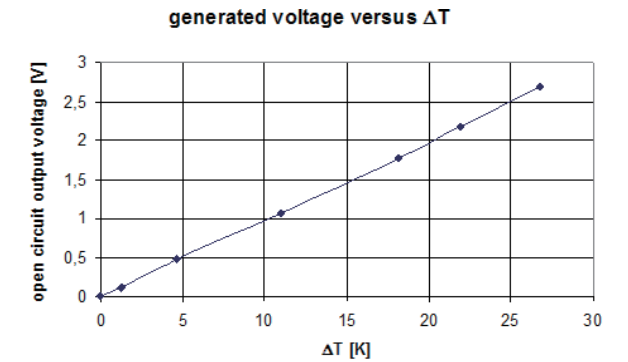


Fig. 13. (Color online) Five samples.



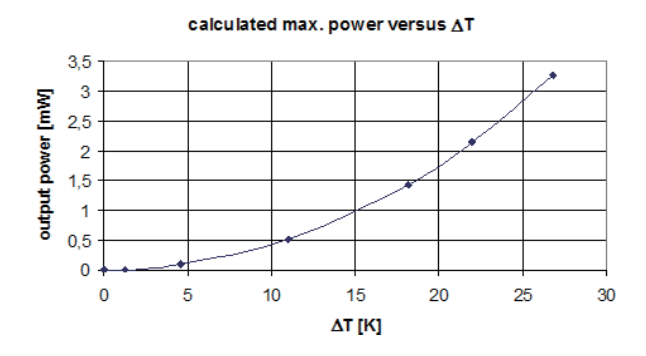


Fig. 14. (Color online) Characteristic curve of MPG-D602.

Table 4 Specifications of Samples B, D, and E.

Specifications of Samples 2, 2, and 2.							
Sample	В	D	Е				
Model number	TEC-127.04	TES1-241.100	TEC-241.10				
Dimension (mm)	$40 \times 40 \times 4.7$	$40 \times 40 \times 2.7$	$50 \times 50 \times 3.9$				
Maximum voltage (V)	15.2	29.2	29.4				
Maximum current (A)	4	10	10				
power (W)	35.6	168.7	168.7				

Table 5 Specifications of Sample C.

Sample	С
Model number	TGM199-1.4-0.8
Dimension (mm)	$40 \times 40 \times 3.2$
Voltage $(T=0)$ (V)	6
Current $(I = 0)$ (A)	3.5
Voltage $(T = 50)$ (V)	4
Current $(I = 50)$ (A)	2.4
Power $(T=0)$ (W)	21.1
Power $(T = 50)$ (W)	9.4
Efficiency $(T=0)$	5.80%
Efficiency $(T = 50)$	3.80%

standard), 199 is the number of thermoelectric elements, 1.4 is the pellet height, and 0.8 is the thickness of the thermoelectric generator module.

Sample D is a thermoelectric cooling module (model number TES1-241.100) with the basic specifications listed in Table 4. TES1 is the thermoelectric generation code (N and P pellet sizes are less than 1 mm), 241 is the number of thermoelectric elements, and 100 A is the maximum operating current.

Sample E is a thermoelectric cooling module (model number TEC-241.10) with the basic specifications listed in Table 4. TEC is the thermoelectric generation code (N and P pellet sizes are greater than 1 mm), 241 is the number of thermoelectric elements, and 10 A is the maximum operating current.

(2) Heater and heating plate

The heater has a power of 500 W and an operating temperature range from ambient temperature (25 °C) to 400 °C. The surface temperature of the heater plate is monitored by a temperature sensing wire. The signal is fed back to the heater to precisely control the heating temperature at all times.

(3) Heat spreader

This is a red copper plate of 5 mm thickness.

(4) Pig skin

(5) Thermometer

Model: 53II, Serial Number: 92950061, Measurement Range: K-type, -200 to +1372 °C Measurement Accuracy: 0.05% + 0.3 °C (0.5 F) Reading

Temperature Sensing Wire: Class I grade wire, with lower resistance and higher conductivity.

(6) Water tank

The tank is constructed from a heat sink as the base and an acrylic frame is used to contain water and ice.

(7) Battery

A button-type rechargeable battery (model no. LIR2477) with a nominal capacity of 180–190 mAh, an operating voltage of 3.6 V, a maximum discharge current of 2C, and a termination voltage of 2.7 V is used. The dimensions are shown in Fig. 15.

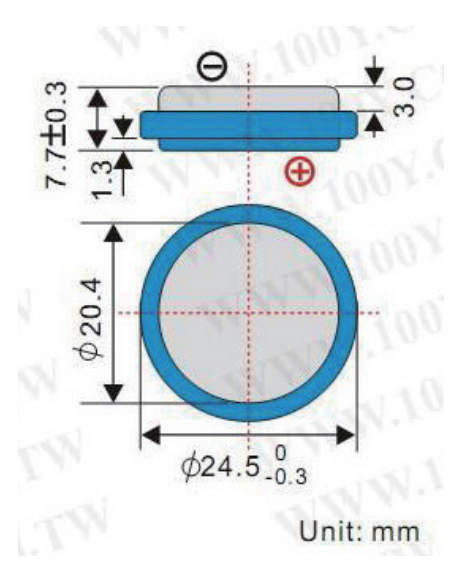


Fig. 15. (Color online) Battery dimensions.

3.3 Circuitry

The voltage and current generated by thermoelectric modules vary depending on their series and parallel arrangements.

- (A) The series connection of thermoelectric modules produces a higher voltage but a lower current, which can provide sufficient voltage to charge the battery.
- (B) The parallel connection of thermoelectric modules produces a higher current but a lower voltage. The circuitry needs a boost circuit to provide enough voltage for battery charging.

3.3.1 Boost circuit

A control IC (model TPS61202DSC)⁽¹⁷⁾ made by Texas Instruments is used in this study. Figure 16 shows the pin diagram of the boost circuit, and the physical circuit is illustrated in Fig. 17.

3.3.2 Charging circuit

We utilized a control IC (model BQ24002PWP)⁽¹⁷⁾ provided by Texas Instruments. The pin diagram is shown in Fig. 18. The IC is a linear charge management device. The package is combined with high-accuracy current and voltage regulation, temperature, or input-power monitoring, charge termination, and charge-status indication. The input voltage can be monitored to qualify charge. The package size is 6.5×4.4 mm.

3.3.3 Discharge circuit

The battery used in this study is LIR2477, with an operating voltage of 3.6 V. When the battery is used for a certain period, its voltage will drop to 2.7 V, which is the termination

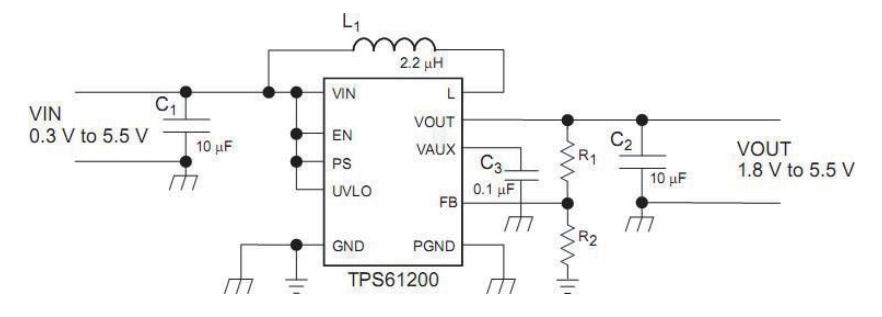


Fig. 16. Pin diagram of boost circuit.

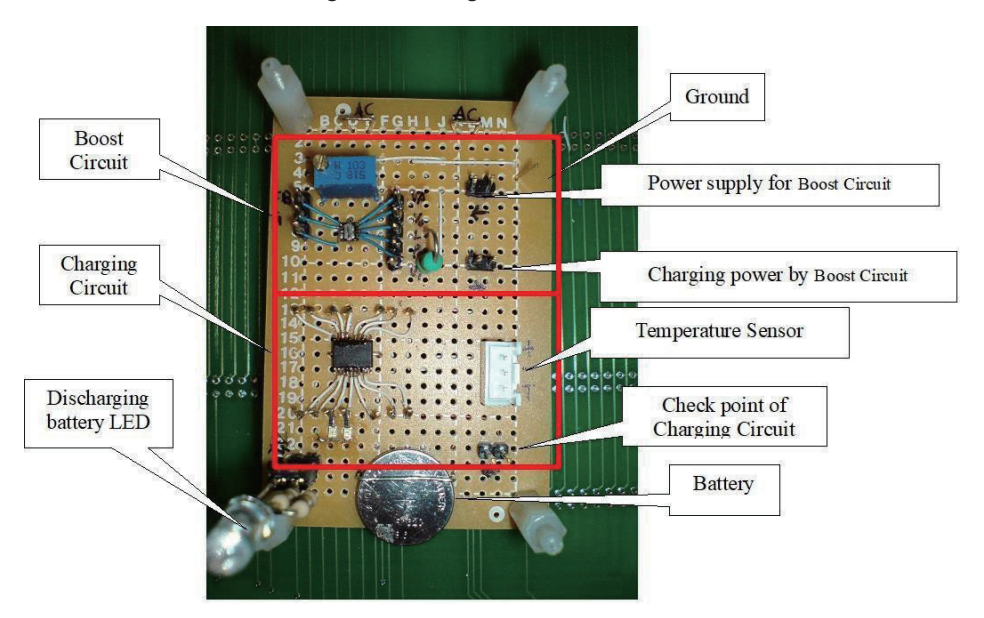


Fig. 17. (Color online) Physical circuit.

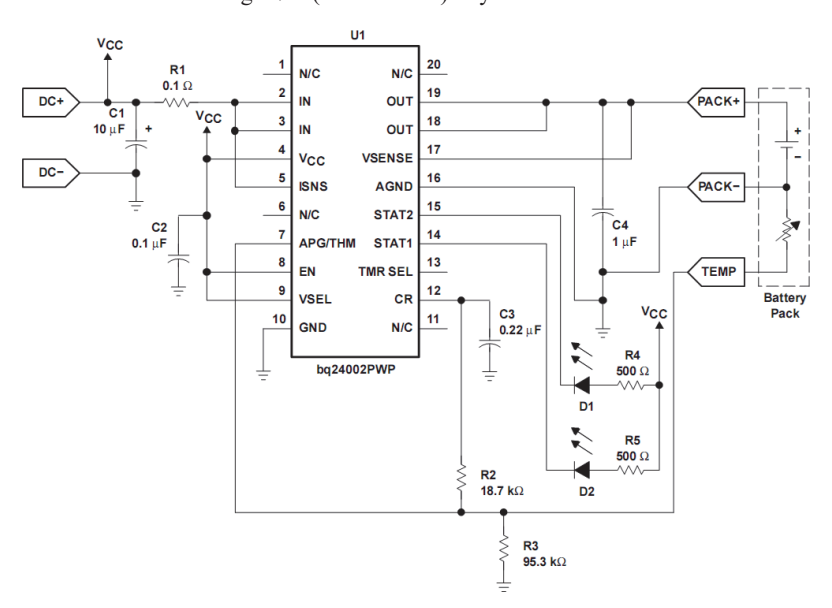


Fig. 18. Pin diagram of BQ24002PWP.

voltage. Continued use beyond this voltage can lead to overdischarge and damage to the battery. The discharge circuit is composed of an LF351 comparator. Figure 19 shows the pin diagram of the LF351 discharge circuit.

3.4 Experimental setup assembly

Figure 20 shows the schematic diagram of the thermoelectric power generation system constructed in this study. The heating plate represents the hypothalamus controlling the human body temperature, the temperature of the heat spreader plate represents the human body temperature, the pig skin simulates the human skin, and the ice—water bath temperature simulates the external ambient temperature of the human skin. The surroundings and the cap of the ice—water mixture tank are covered with a rubber foam material that can lock large amounts of air within pores to prevent temperature loss to the environment. The optimal thermal insulation effect is achieved in the experimental environment.

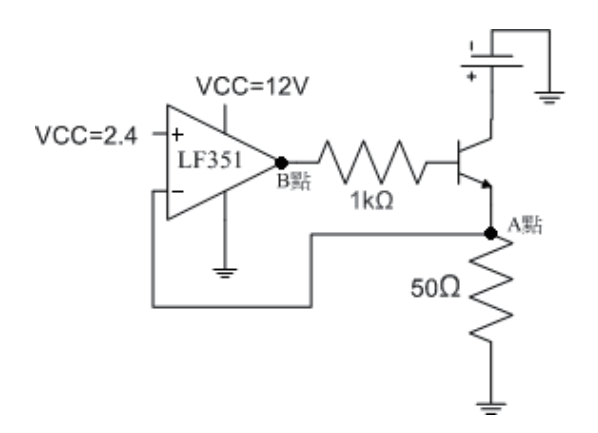
Thermoelectric modules are arranged on the surface of the heat spreader plate without voids between them. One temperature sensor is placed between each of the three thermoelectric modules and the heat spreader plate. After covering the whole heat spreader plate with pig skin, a water bath containing an ice—water mixture is placed on top of the pig skin. Then, the setup of the thermoelectric generation system is finished and is shown in Fig. 21.

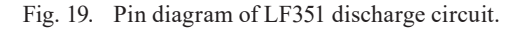
3.5 Experimental procedure

This experiment consisted of two procedures: (1) voltage and current measurement and (2) charging experiment.

(1) Voltage and current measurement procedure

In this study, this procedure was used to measure the voltage and current data corresponding to the temperature gradient between the cold and hot ends of the thermoelectric power generation system. The procedure is shown in Fig. 22 and explained below.





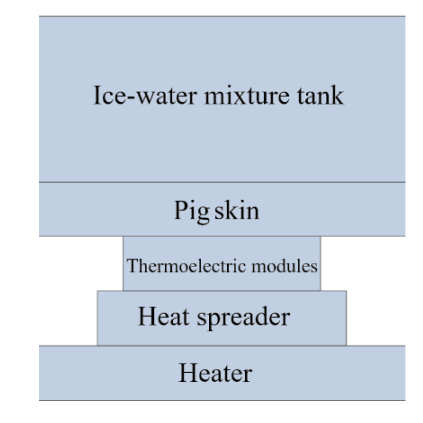


Fig. 20. (Color online) Schematic diagram of thermoelectric charging module system.

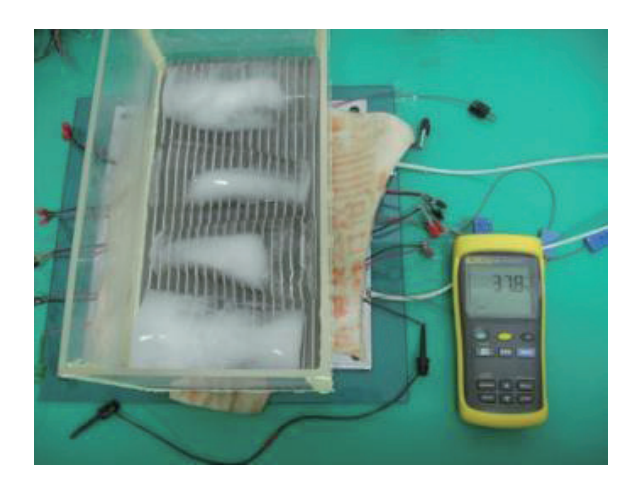
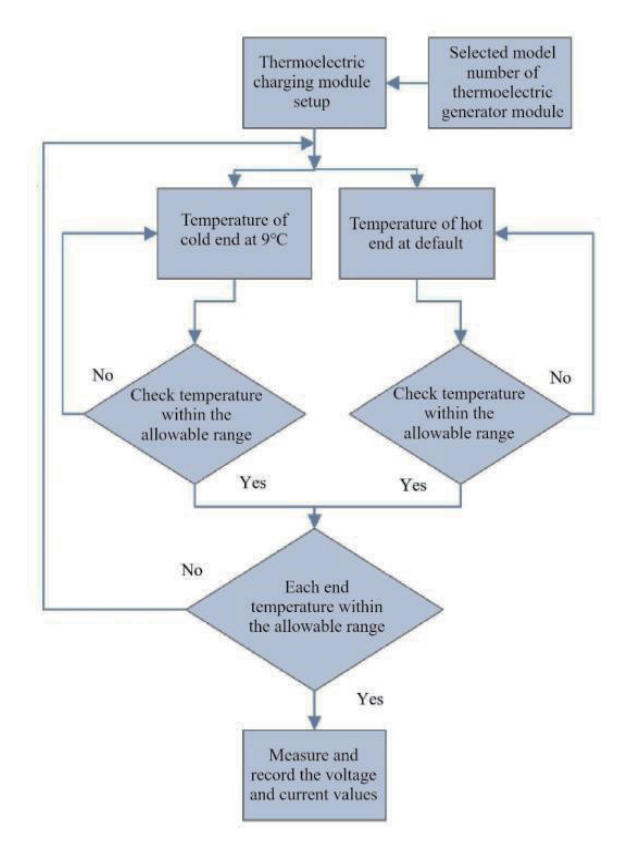


Fig. 21. (Color online) Setup of thermoelectric power generation system.



 $Fig.\ 22.\ \ (Color\ on line)\ Flow chart\ for\ voltage\ and\ current\ measurements.$

- (a) Select the thermoelectric module model.
- (b) Complete the setup of the thermoelectric power generation module.
- (c) Adjust the hot- and cold-end temperatures to their preset values (cold end at 9 °C), allowing for a temperature variation range of ± 1 °C at each end over time.

(d) When the temperature values at each end are within the allowable range, use a multimeter to measure and record the voltage and current values of the thermoelectric power generation system.

(2) Charging experiment procedure

This procedure was used to record the relevant data for charging the battery with the electrical energy generated by the thermoelectric power generation system. The procedure is shown in Fig. 23 and the details are as follows.

- (a) Select the thermoelectric module model.
- (b) Complete the setup of the thermoelectric power generation module.
- (c) Adjust the cold end temperature to 9 °C and the hot end temperature to 37 °C, allowing for a variation range of ± 2 °C.
- (d) Check the temperature at each end every minute to ensure that it remains within the allowable range.
- (e) If the temperature at each end is within the allowable range, measure the voltage and current values of the thermoelectric power generation module system and compare them with the data recorded in the voltage and current measurement procedure. If the data is abnormal, check for any setup defects in the thermoelectric charging system first and readjust the hotand cold-end temperatures.
- (f) When all temperature values are adjusted and maintained within the range, begin charging the battery immediately and record the relevant data during charging (e.g., voltage, current, and temperature).

During the process, check the temperature values of each sensor every minute to ensure that they are still within the allowable range. If they exceed the range, charging must be paused immediately, and each temperature must be adjusted back within the range before resuming the charging process until the limited charging time or full charge is reached

4. Results and Discussion

4.1 Effects of pig skin on experimental results

4.1.1 Effect of pig skin thickness

Pig skin is often used to simulate human skin owing to its skin tissue similarities.⁽¹⁸⁾ The pacemakers are implanted between the subcutaneous fat layer and the muscle layer below the shoulder blade. The 3- and 5-mm-thick pig skin samples were pressed under an ice—water mixture tank and the inner temperature of the samples was measured for a certain period.

The results showed that the inner temperature of both pig skin thicknesses stabilized at 9 °C. This indicates that the pig skin thickness does not affect the results of this study.

4.1.2 Effect of pig skin area

Completely covering both the thermoelectric modules and the heating plate with pig skin will prevent their temperatures from being affected by the external environment. However, it is not

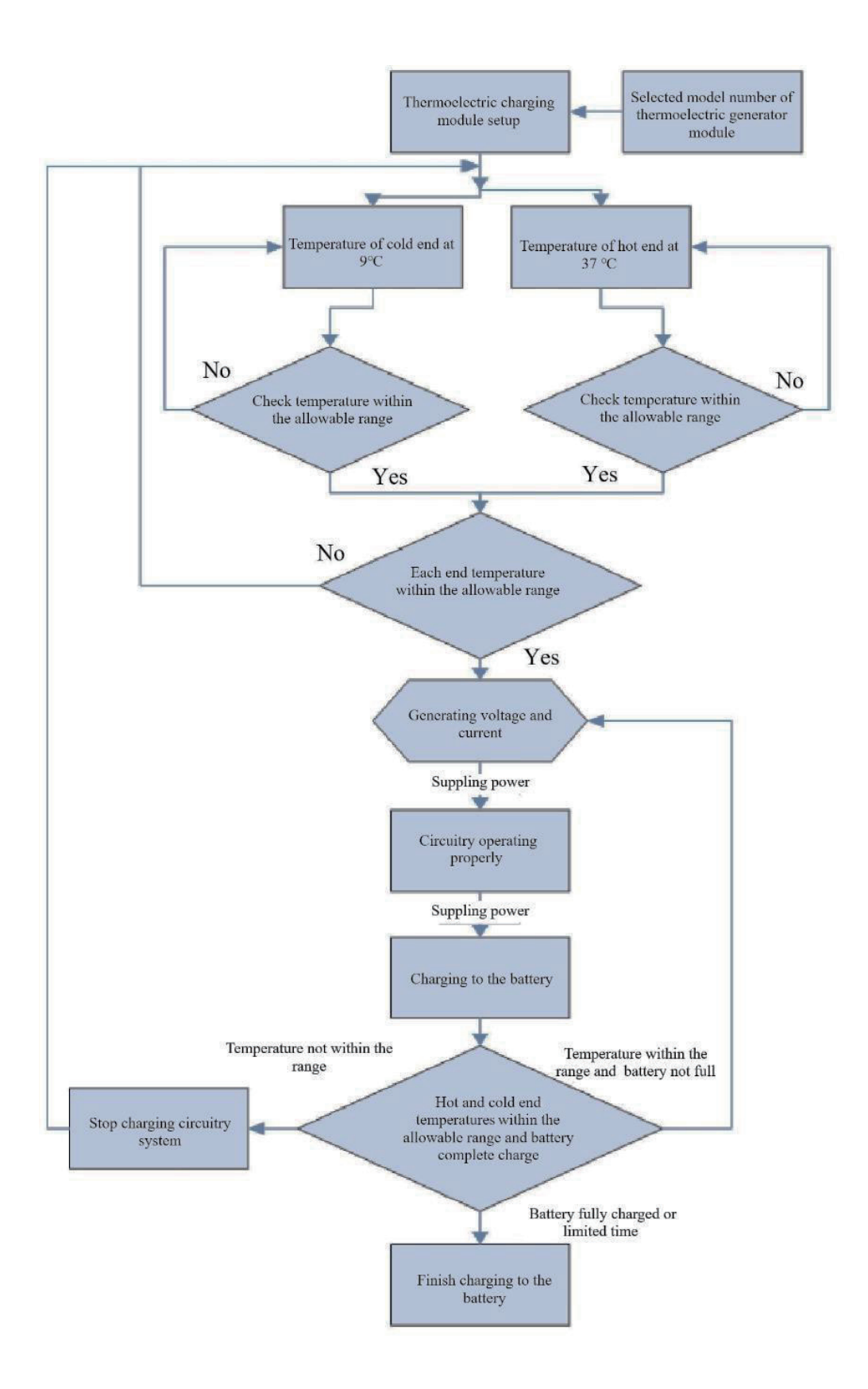


Fig. 23. (Color online) Flowchart for charging.

easy to obtain such a large area of pig skin (matching the 280 × 280 mm² heating plate). The covering method shown in Fig. 24 was adopted. In Fig. 24, the blue area represents the portion covered by the pig skin, and the red area indicates the uncovered part of the heating plate. The heating plate was not covered entirely, and the uncovered (red) portion had negligible impact on the temperature of the heat spreader plate.

4.1.3 Effect of pig skin humidity

The surface temperature of the heating plate is significantly higher than the ambient temperature. The pig skin can lose moisture and become dry as a result of continuous heating. Thus, the pig skin had to be replaced every 2 h during the experiment.

4.2 Testing of different power generation modules and arrangement methods

The power generation characteristics of various samples were compared through the following experiments to determine the suitable arrangement.

(1) Single Module Test

Single module tests of Samples B, C, D, and E with voltage and current measurements were performed following the procedure described in Sect. 3.5. The experimental results are presented in Table 6 and plotted for comparison. As shown in Fig. 25, Sample D generated higher voltage values. Figure 26 indicates that the current of Sample E surpassed those of Sample D at temperatures above 42 °C. From the preliminary results, it can be concluded that Samples B and C had poorer power generation performance.

(2) Two-module Series Test

Two of the same samples are connected in series and the voltage and current are measured as described in Sect. 3.5 to verify the accuracy of the single sample data. The test data are presented in Table 7 and plotted in Figs. 27 and 28. Figure 27 shows that Sample D generates higher voltage

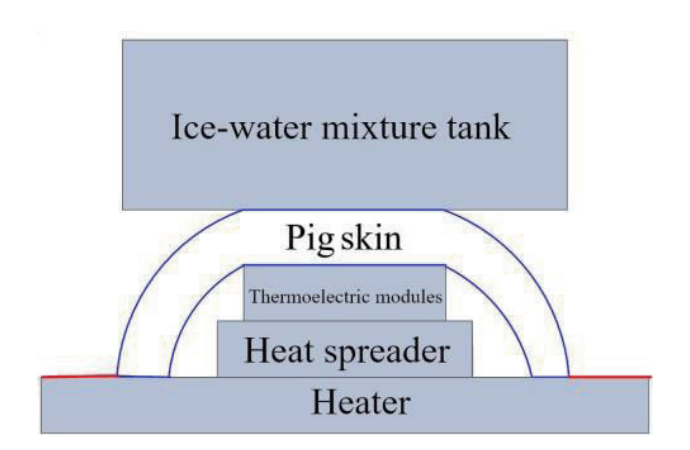


Fig. 24. (Color online) Schematic diagram of pig skin coverage area.

Table 6
Single module test results of thermoelectric modules.

Therm module	oelectric e	Sam	ple B	Sam	ple C	Sam	ple D	Sam	ple E
Cold e	nd Hot end	Voltage	Current	Voltage	Current	Voltage	Current	Voltage	Current
(°C)	(°C)	(V)	(mA)	(V)	(mA)	(V)	(mA)	(V)	(mA)
9	30	0.23	24	0.09	12	0.5	34	0.31	32
9	32	0.24	26	0.11	14	0.63	40	0.36	39
9	34	0.29	28	0.121	15	0.67	44	0.38	40
9	36	0.3	33	0.128	16	0.73	47	0.42	44
9	38	0.34	36	0.13	17	0.78	50	0.46	46
9	40	0.36	38	0.134	18.7	0.81	53	0.53	52
9	42	0.38	40	0.144	20	0.89	54	0.55	56
9	44	0.39	42	0.157	21.6	0.93	58	0.6	61
9	46	0.45	48	0.161	22	0.95	60	0.63	63

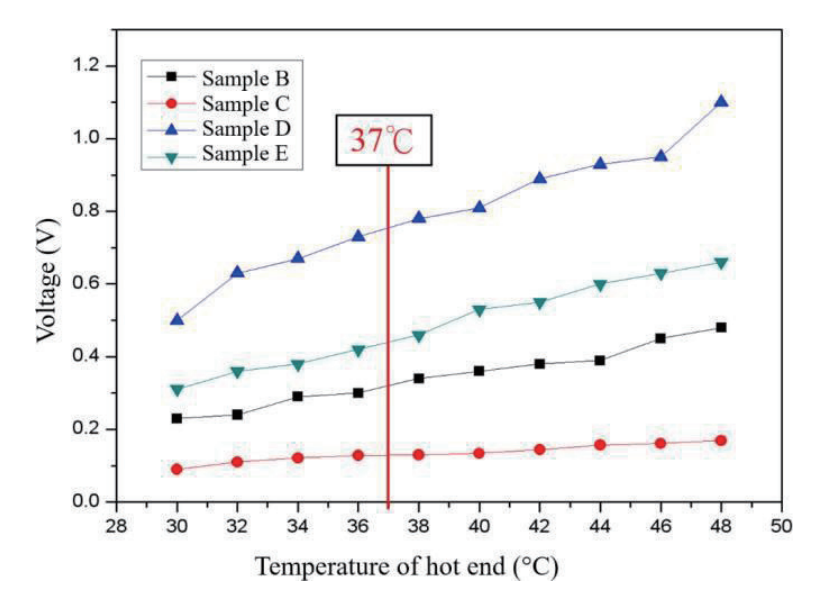


Fig. 25. (Color online) Voltage obtained by single module testing.

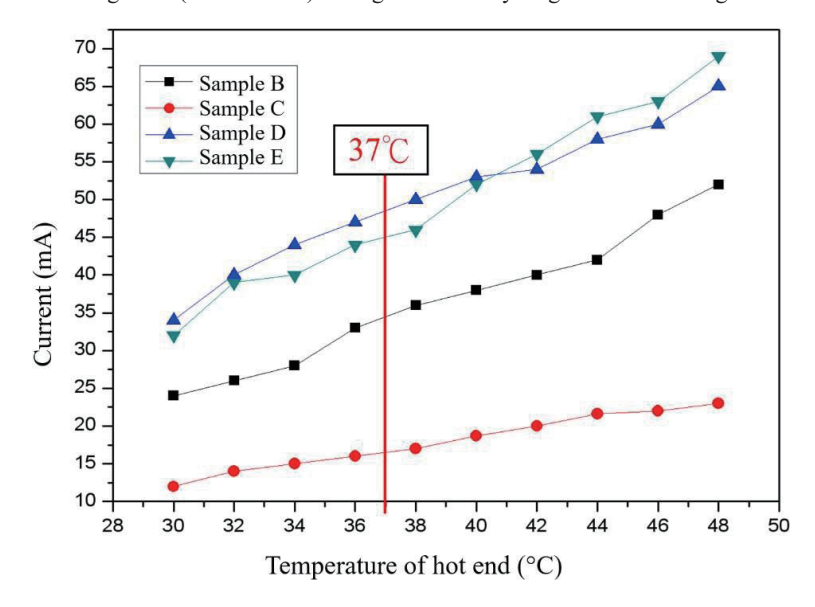


Fig. 26. (Color online) Current obtained by single module testing.

Table 7
Two-module series test results of thermoelectric modules.

Thermo	electric	Sam	ple B	Sam	ple C	Sam	ple D	Sam	ple E
Cold end	Hot end	Voltage	Current	Voltage	Current	Voltage	Current	Voltage	Current
(°C)	(°C)	(V)	(mA)	(V)	(mA)	(V)	(mA)	(V)	(mA)
9	30	0.45	34	0.18	21	0.98	38	0.5	40
9	32	0.49	37	0.21	23	1.23	46	0.67	51
9	34	0.55	40	0.23	23	1.32	50	0.72	54
9	36	0.6	46	0.24	26	1.36	53	0.79	59
9	38	0.63	50	0.26	29	1.47	55	0.96	70
9	42	0.74	56	0.29	32	1.68	63	1.1	79
9	44	0.79	58	0.32	35	1.86	68	1.21	87
9	46	0.87	64	0.34	36	1.92	69	1.25	90
9	48	0.96	68	0.34	37	2.1	75	1.34	94

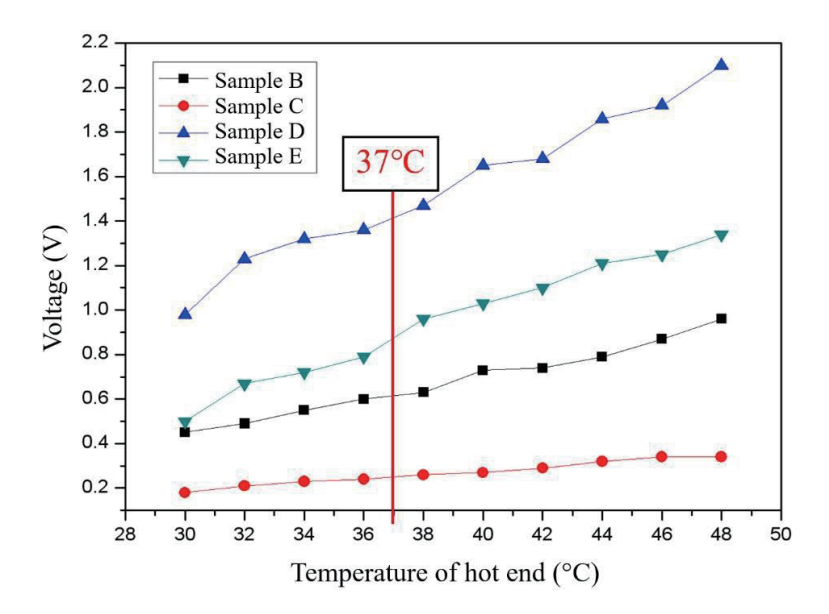


Fig. 27. (Color online) Voltage obtained by two-module series testing.

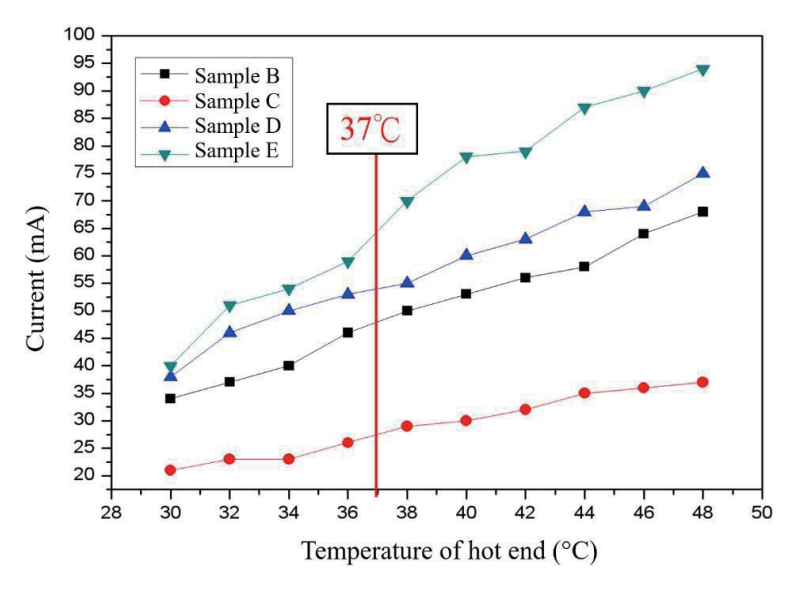


Fig. 28. (Color online) Current obtained by two-module series testing.

values, exceeding 1 V, whereas the Sample E voltage was slightly lower. The voltages of Samples B and C remained low. Figure 28 shows that Sample E generated a higher current than Sample D, and Samples B and C still had low current values. On the basis of the results, Samples B and C were eliminated.

If the voltage and current values generated by thermoelectric modules are very low, they cannot drive a circuit to charge a battery. In this case, parallel connection is needed to increase the current output, and series connection is used to raise the voltage output.

(3) Two-series, Three-parallel Test for Samples D and E

This test involved an arrangement where two thermoelectric modules were connected in series to form a group, and then three groups were connected in parallel, as shown in Fig. 29.

Table 8 shows the results obtained following the voltage and current measurement procedure described in Sect. 3.5, which were then plotted for comparison. Figures 30 and 31 clearly show

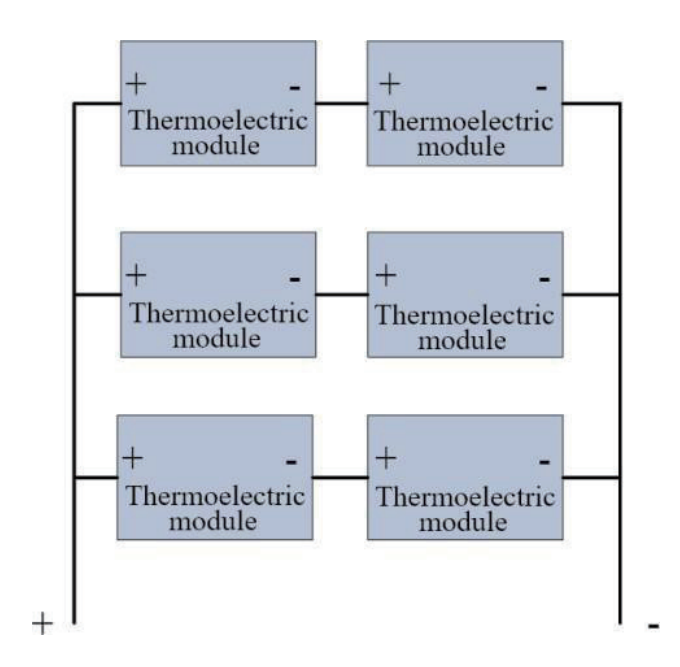


Fig. 29. (Color online) Two-series, three-parallel arrangement.

Table 8 Voltage and current of two-series, three-parallel arrangement.

Thermoelectric	module	Sam	ple D	Sample E		
Cold end (°C)	Hot end (°C)	Voltage (V)	Current (mA)	Voltage (V)	Current (mA)	
9	30	0.819	60.8	0.49	50	
9	32	0.929	67.2	0.52	54	
9	34	1.093	75.5	0.58	58	
9	36	1.184	83.2	0.64	64	
9	38	1.217	84.4	0.67	72	
9	40	1.308	87.9	0.72	81	
9	42	1.437	95.2	0.8	87	
9	44	1.567	103.8	0.84	92	
9	46	1.665	109.5	0.86	96	
9	48	1.72	112.8	0.94	98	

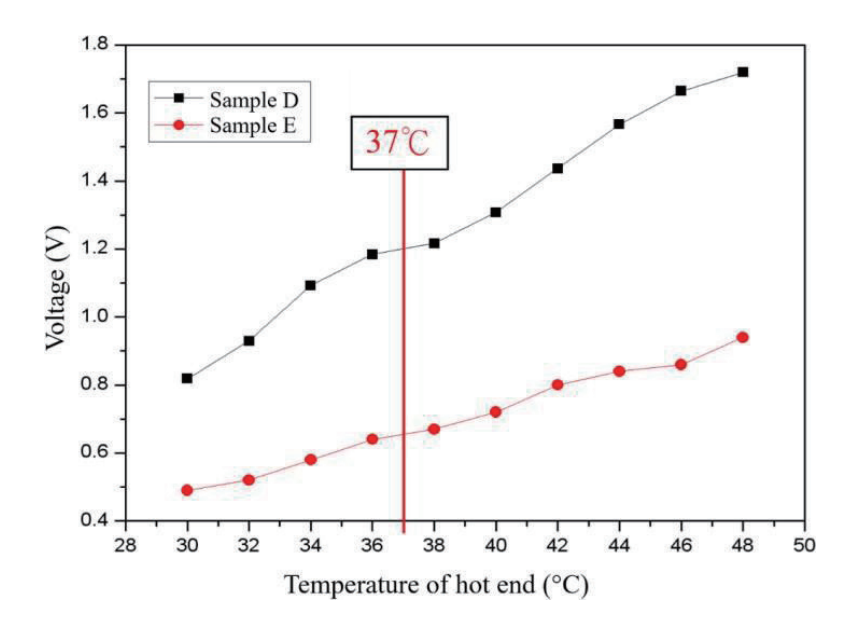


Fig. 30. (Color online) Output voltage for two-series, three-parallel arrangement.

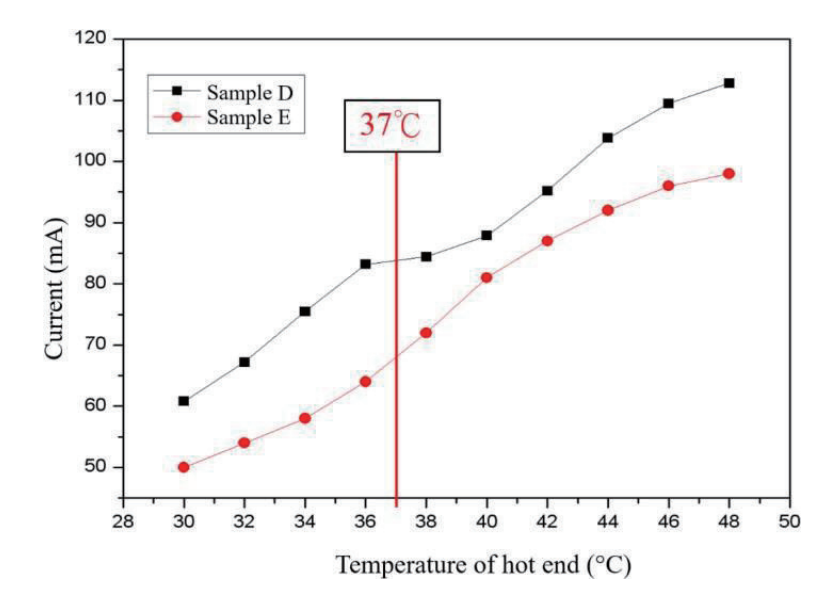


Fig. 31. (Color online) Output current for two-series, three-parallel arrangement.

that both the voltage and current of Sample D were higher than those of Sample E. At a hot-end temperature of 37 °C , the voltage ranged of Sample D from 1.184 to 1.217 V, and its current ranged from 83.2 to 84.4 mA. However, from the combination, it was found that the battery could not be charged, leading to the rejection of the two-series, three-parallel arrangement. Both Samples D and E have 241 thermoelectric elements. The only difference lies in the size of the semiconductor crystal grains. Sample D has crystal grains smaller than 1 mm and is primarily used in cooling applications where it bears a lower current of 4 mA. Sample E has crystal grains larger than 1 mm and handles a higher current of 10 mA in cooling applications. The results

indicate that for the same number of elements, modules with smaller crystal grains have higher power generation efficiency. The measurements confirmed that the electrical energy produced by thermoelectric cooler modules is comparable to that produced by thermoelectric generation modules. On the basis of the above, Sample D was selected as the thermoelectric module for the thermoelectric power generation system. However, to achieve maximum power generation efficiency, a suitable arrangement that meets the minimum power requirements of the circuit to charge the battery must be found.

(4) Four Series-parallel Arrangement Tests for Sample D

Figure 32 illustrates four different arrangement methods for Sample D. Table 9 presents the voltage and current power generation results for the four arrangements. Figures 33 and 34 show

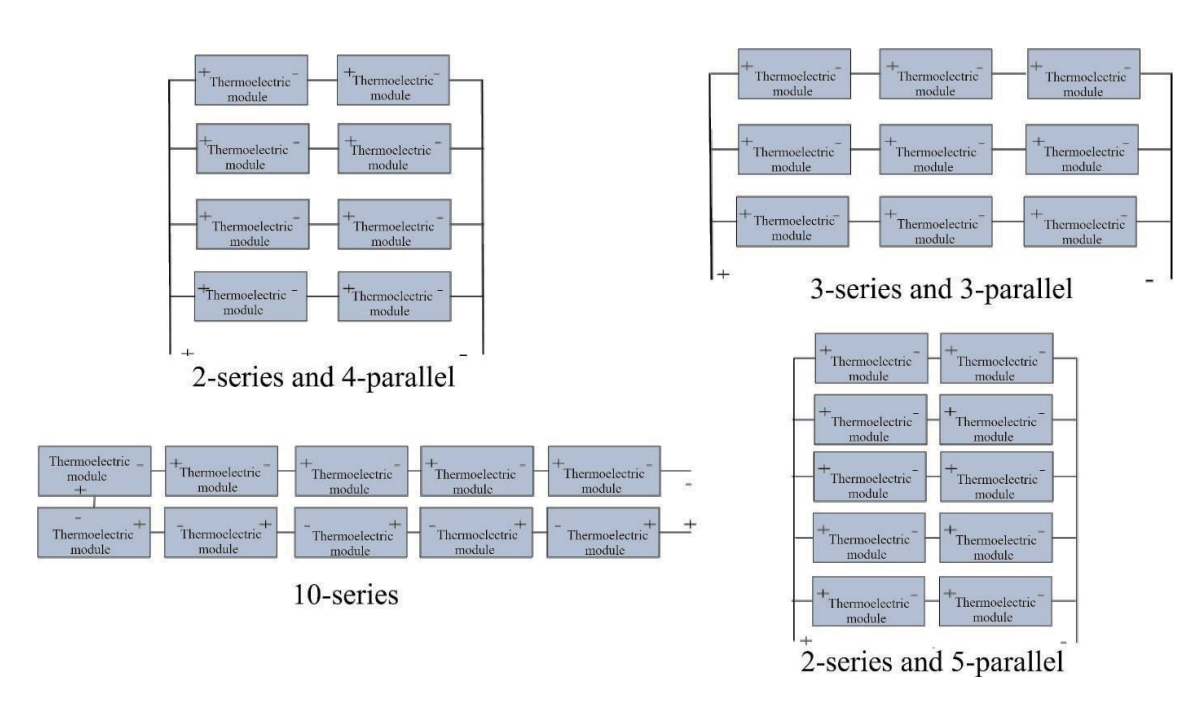


Fig. 32. (Color online) Four arrangements of Sample D.

Table 9
Output voltage and current for four arrangements of Sample D.

Thermoel	ectric	Two-s	series,	Three	-series,	Ton	series	Two-s	series,
module		four-p	arallel	three-1	parallel	1011-8	SCIICS	five-p	arallel
Cold end	Hot end	Voltage	Current	Voltage	Current	Voltage	Current	Voltage	Current
(°C)	(°C)	(V)	(mA)	(V)	(mA)	(V)	(mA)	(V)	(mA)
9	30	0.55	53	0.91	54	4.17	36.2	0.99	87
9	32	0.75	74	1.02	60	4.5	41.7	1.06	98
9	34	0.83	82	1.08	63	4.7	42.4	1.14	104
9	36	0.87	87	1.16	67	5.34	45.2	1.2	112
9	38	1.03	92	1.27	73	5.68	47.1	1.28	114
9	40	1.11	96	1.34	78	5.74	47.5	1.36	116
9	42	1.18	106	1.41	81	6.1	52	1.41	121
9	44	1.26	115	1.48	85	6.7	54.1	1.48	123
9	46	1.35	122	1.55	89	7.26	58.7	1.53	128
9	48	1.44	132	1.63	91	7.33	62	1.59	131
		-							

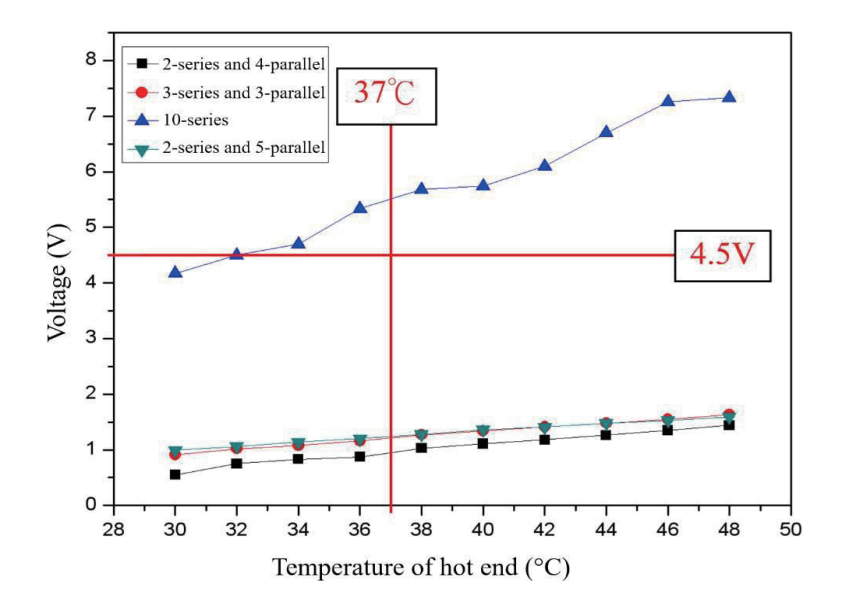


Fig. 33. (Color online) Output voltage for four arrangements of Sample D.

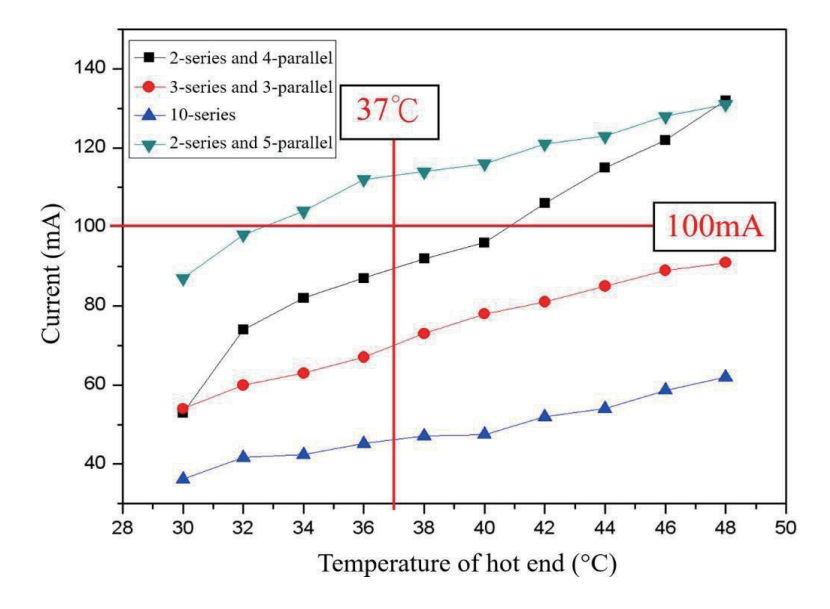


Fig. 34. (Color online) Output current for four arrangements of Sample D.

that the ten-series arrangement yielded the highest voltage values, whereas the two-series, five-parallel arrangement resulted in the highest current values. When nine Sample D modules were connected in series and the hot side temperature was 37 °C (human body temperature), the output voltage was above 4.5 V (calculated by interpolation).

However, the current was around the critical activation threshold of 42 mA for the circuit. The output of ten Sample D modules in series was slightly higher than 4.5 V and 42 mA, which is sufficient to drive the charging circuit. With nine Sample D modules in series, minor changes in the temperature gradient of the thermoelectric power generation system can lead to

discontinuous charging. With ten Sample D modules in series, since the generated voltage and current are slightly higher than the circuit's activation voltage and current, discontinuous charging can be avoided. From the results, it is clear that the minimum number of thermoelectric modules for a series arrangement is ten.

Figure 34 shows that the current generated by the two-series, five-parallel arrangement is higher than that of the ten-series arrangement, but the voltage is lower. When the thermoelectric generation system produces low voltage and high current, a boost converter is required to increase the output voltage before it can drive the charging circuit to charge the battery. Since the activation voltage and current of the charging circuit are 0.3 V and 100 mA, respectively. At the hot end temperature of 37 °C, the two-series, four-parallel arrangement produced a voltage between 0.78 and 1.03 V and a current between 87 and 92 mA, leading to discontinuous charging. The two-series, five-parallel arrangement produced a voltage between 1.2 and 1.28 V and a current between 112 and 114 mA. It can be concluded that the minimum number of thermoelectric modules for a parallel arrangement is ten.

From the results, it is evident that both the ten-series and two-series, five-parallel arrangements can generate sufficient voltage and current to charge a battery. In this study, we will further investigate which of the two arrangements offers superior thermoelectric power generation performance.

(1) Two-series, five-parallel arrangement

The boost converter circuit is needed by the arrangement. Following the charging procedure detailed in Sect. 3.5, the generated voltage and current at various hot end temperatures were measured, with the results presented in Table 10. When the hot end temperatures were 30 and 32 °C, the voltage and current produced by the thermoelectric generation system are insufficient to drive the charging circuit. No relevant data are available for the temperatures. The hot end temperature must exceed 34 °C for the boost converter circuit to operate normally and charge the battery. The result represents the minimum charging temperature for the two-series, five-parallel arrangement, and the thermoelectric generation system supplies a current of 104 mA to the boost converter circuit. After consumption by the boost converter, 2.27 mA remains available

Table 10
Output voltage and current for two-series, five-parallel arrangement.

	0			_				
Two-ser	ies, five-parallel	Thermoelectric module (open loop)		Input of charging circuit		Battery		
Cold end	d (°C) Hot end (°C)	Voltage (V)	Current (mA)	Voltage (V)	Current (mA)	Voltage (V)	Current (mA)	
9	30	0.99	87	5.086				
9	32	1.06	98	5.086				
9	34	1.14	104	5.086	2.27	3.1	1.76	
9	36	1.2	112	5.086	2.56	3.1	1.81	
9	38	1.28	114	5.086	2	3.1	1.89	
9	40	1.36	116	5.086	1.99	3.2	1.96	
9	42	1.41	121	5.086	1.94	3.2	2.9	
9	44	1.48	123	5.086	1.99	3.2	3.17	
9	46	1.53	128	5.086	1.95	3.2	3.6	
9	48	1.59	131	5.086	1.98	3.19	1.91	

for the charging circuit. With further consumption of the charging circuit, only 1.76 mA is left to charge the battery. When the hot end temperature reaches 37 °C, the thermoelectric generation system applies 112–114 mA to the boost converter circuit. After consumption by the boost converter, 2.56–2 mA remains for the charging circuit. Following further consumption by the charging circuit, 1.81–1.89 mA remains to charge the battery. The result indicates that while the boost converter circuit increases the voltage signal from the thermoelectric generation module, enabling the charging circuit to charge the battery, it consumes a large amount of current. The actual current supplied to the battery for charging is only 1.81–1.89 mA, which is approximately 1.64% of the current generated by the thermoelectric power generation module, with the remaining 98.36% of the current being consumed by the circuit.

(2) Ten-series arrangement

Using the ten-series arrangement and following the charging procedure detailed in Sect. 3.5, the generated voltage and current values at various hot end temperatures were measured, with the results being presented in Table 11. When the hot end temperatures are 30 and 32 °C, the voltage and current produced by the thermoelectric power generation system are insufficient to drive the charging circuit; hence, no relevant data are available. The hot end temperature must exceed 34 °C for the thermoelectric generation module to produce sufficient voltage and current to activate the charging circuit; this represents the minimum charging temperature for the tenseries arrangement. As shown in Table 11, when the hot end temperature is 37 °C, the thermoelectric generation system produces a voltage of 5.37–5.68 V and a current of 45.2–47.1 mA to supply the charging circuit. After consumption by the charging circuit, the charging current available to the battery is 12–13.9 mA, which is approximately 28% of the current generated by this arrangement's power generation module, with the remaining 72% of the current being consumedby the circuit.

The results indicate that the two-series, five-parallel arrangement consumes more current than the ten-series arrangement. The two-series, five-parallel arrangement added a boost converter circuit, resulting in 98.36% of the electrical energy generated by the thermoelectric generation system being consumed by the circuit, with only 1.64% remaining to charge the battery. In contrast, with the ten-series arrangement, 72% of the electrical energy generated by

Table 11
Output voltage and current for ten-series arrangement.

Ten-series		Thermoelectric module (open loop)		Input of cha	arging circuit	Battery		
Cold end (°C) Hot end (°C)	Voltage (V)	Current (mA)	Voltage (V)	Current (mA)	Voltage (V)	Current (mA)	
9	30	4.17	36.2					
9	32	4.5	41.7					
9	34	4.9	42.4	3.1	15.2	2.56	11.1	
9	36	5.34	45.2	3.711	16.4	2.9	12	
9	38	5.68	47.1	3.917	17.7	3.08	13.9	
9	40	5.74	47.5	3.923	19.2	3.2	15.2	
9	42	6.1	52	3.911	23.2	3.52	17.2	
9	44	6.7	54.1	4.32	24.8	3.6	18.4	
9	46	7.26	58.7	3.956	25.5	3.65	19.6	
9	48	7.33	62	4.22	26.4	3.74	20.4	

the thermoelectric generation system is consumed by the circuit, with the remaining 28% available to charge the battery. To achieve the same charging result, the charging time for the two-series, five-parallel arrangement would be 17 times longer than that for the ten-series arrangement. It can be concluded that the ten-series arrangement is the optimal configuration among the various thermoelectric module arrangements investigated in this study.

4.3 Experimental results

Tables 2 and 3 show that the current consumptions of the implanted pacemaker in the sensing and pacing modes are 12 and 21 µA, respectively. Table 12 lists the pacemaker extended operating time after the batteries were charged by the thermoelectric charging system for different durations in this study. For example, the battery gains 14.784 mAh after 1 h of charging, which can extend the pacemaker's operation in the sensing and pacing modes by 1232 h (51.3 days) and 704 h (29.3 days), respectively. Figure 35 is presented to demonstrate the extended operating time in both the pacing and sensing modes vs charging time. The results of this study indicate that charging the implantable pacemaker battery with the thermoelectric device for various times can extend the number of pacemaker working days. Moreover, the power

Table 12 Estimated extended operating time of pacemaker after charging.

Charging time (h)	Stone on compaits (m. A.b.)	Extended operating time (day)			
	Storage capacity (mAh) —	Pacing mode	Sensing mode		
1	14.784	29.3	51.3		
1.5	19.167	38	66.6		
2	34.235	67.9	118.9		
8.35	150.773	299.2	523.5		

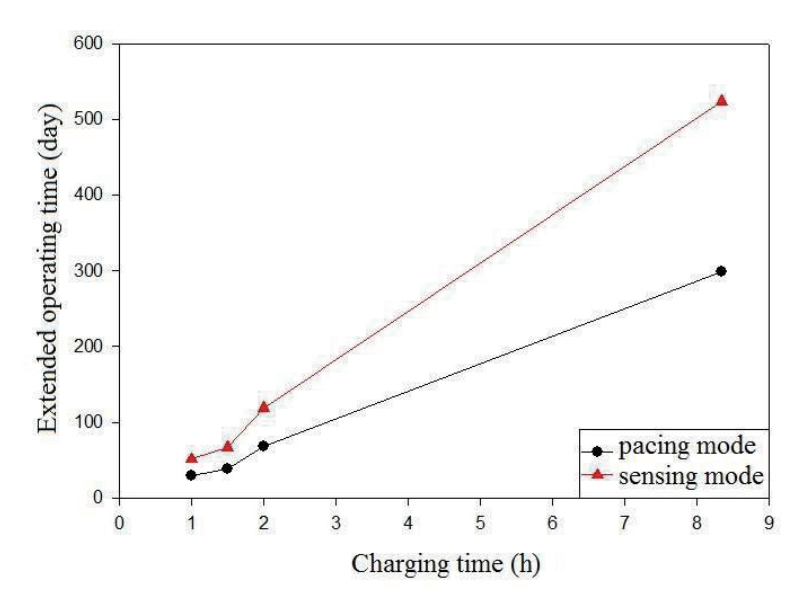


Fig. 35. (Color online) Extended operating time of both pacing and sensing modes vs charging time.

generation area of 160 cm² is divided into two parts of 80 cm² (about 8.9×8.9 cm) each. One is implanted under the scapula on one side and the other is implanted also under the scapula on the other side. When ice packs were applied to both scapular areas, the thermoelectric charging system could take effect.

4.4 Discussion on improving the performance of the thermoelectric charging system

The thermoelectric charging system generates electrical energy on the basis of a temperature gradient, and the energy is then stored in the battery. With the inhomogeneity of surface temperature, the performance of the thermoelectric power module would decrease. The temperature sensor was placed between the thermoelectric module and the heat spreader, resulting in a void between them, which would decrease the power generation of the thermoelectric generation system.

As shown in Table 6, under the same conditions, the power generation voltage of Sample D is more than five times that of Sample C. An excellent thermoelectric module can reduce the generation module area or increase the generation power. In addition, the circuit consumes power, which can reduce the energy stored in the battery by the thermoelectric module. Regarding the battery charging of implanted pacemakers, the efforts required for a thermoelectric charging system will be as follows.

- (1) The generation voltage and current should be high with a small temperature gradient.
- (2) The thermoelectric module should be small.
- (3) The circuit consumption should be low.
- (4) The capacity of the rechargeable battery should be large.
- (5) The charging speed should be high.
- (6) The cost should be inexpensive.

5. Conclusions and Future Works

5.1 Conclusions

In this study, we experimentally investigated the power generation effects of various thermoelectric module models and different arrangements. Table 12 shows that charging the implanted pacemaker battery for different durations can extend the number of operation days of the pacemakers. Charging durations of 1, 1.5, and 2 h can extend the operational time of the battery of an implanted pacemaker in pacing mode for 29.3, 38, and 67.9 days, respectively. For the 180 mAh battery, charging time from zero to full electric state is 8.35 h, which can extend the use time to 299.2 days.

The thermoelectric generator module can be used to recharge the implanted pacemaker's battery, and it can effectively resolve the issue of pacemaker failure resulting from power shortage. Patients need to undergo only a single implantation surgery and a second surgery to replace the battery because of power shortage can be avoided, which will reduce infection and

risk during the surgery of the patient, which is of great benefit to the patient. Moreover, the risk of a second medical procedure is eliminated and additional medical expenses are avoided.

5.2 Future works

Our future research works are as follows.

- 1. With the improvement of the technology, thermoelectric modules with high conversion efficiency can be developed and the generation area can be significantly reduced.
- 2. The improved circuit design can reduce the circuit power consumption using semiconductor manufacturing technology. The electrical energy generated by the thermoelectric module can be applied more effectively.
- 3. After Phase 2 animal experiments and related issue discussions in the future, we expect to enter Phase 3 human implantation.

References

- 1 A. S. Scott, A. A. Christopher, and L. A. Terrence: J. Power Sources 180 (2008) 657.
- 2 J. G. Noudem, S. Lemonnier, M. Prevel. E. S. Reddy, E. Guilmeau, and C. Goupil: J. European Ceramic Society 28 (2008) 41.
- 3 L. Vladimir, T. Tom, F. Paolo, and V. H. Chris: IEEE Sens. J. 7 (2007) 650.
- 4 J. Weber, K. Potje-Kamloth, F. Haase, P. Detemple, F. Volklein, and T. Doll: Sens. Actuators, A 132 (2006) 325.
- 5 M. Hasebe, Y. Kamikawa, and S. Meiarahi: Int. Conf. Thermoelectrics (2006) 697.
- 6 R. Frank and M. Ralf: Sens. Actuators, B 123 (2007) 413.
- 7 M. Shiozaki, S. Sugiyamd, N. Watanabe, H. Ueno, and K. Itoigawa: Proc. 19th IEEE Int. Conf. Micro Electro Mechanical Systems (IEEE 2006) 946–949.
- 8 J. Yu, H. Zhao, and K. Xie: Cryogenics 47 (2007) 89.
- 9 M. Daniel, A. Y. Jose, S. Joordi, T. Antoni, J. Miguel, and A. C. Juan: IEEE Trans. Instrumentation and Measurement **54** (2005) 1548.
- 10 D. M. Rowe and G. Min: IEE Proc. Sci. Meas. Technol. 143 (1996) 351.
- 11 D. M. Rowe and G. Min: J. Power Sources **73** (1996) 193.
- 12 Abbott. http://www.sjm.com
- 13 K. A. Ellenbogen, G. N. Kay, and B. L. Wilkoff: Clinical Cardiac Pacing and Defibrillation (W. B. Saunders, Philadephia, 2000) 2nd ed. p. 167.
- 14 M. Forde and P. Ridgely: The Biomedical Engineering Handbook (Wiley, New York, 2000) Chap. 77.1.
- 15 D. D Pollock: Thermocouples: Theory and Properties (CRC press Int, 1991) 1st ed. 6, ISBN 0-8493-4243-0.
- 16 Micropelt company. http://www.micropelt.com/
- 17 Texas Instruments company. http://www.ti.com/
- 18 K. Inoue, K.Shiba, E. Shu, K. Koshiji, K. Tsukahara, T. Oh-Umi, T. Masuzawa, E. Tatsumi, Y. Taenaka, and H. Takano: American Society for Artificial Internal Organs 44 (1998) 841.

About the Authors

Shang-Kuo Yang received his B.S. degree in 1982 and his M.S. degree in 1985 in automatic control engineering from Feng Chia University, and his Ph.D. degree in mechanical engineering in 1999 from National Chiao Tung University, Taiwan. From 1985 to 1991, he was an assistant researcher and an instrumentation system engineer of the Flight Test Group, Aeronautic Research Laboratory, Zhong Shan Institute of Science and Technology, Taiwan. Since 1991, he has been with the Department of Mechanical Engineering at National Chin Yi University of

Technology, Taiwan. His research interests are in reliability engineering, data acquisition system, biomedical engineering (cardiac pacemaker, patient nursing monitoring, otolith restoration, and drunk- driving prevention), and automation. (skyang@ncut.edu.tw)

Bei-Fu Ou received his B.S. and M.S. degrees in mechanical engineering in 2006 and 2009 from Ya Dong University of Technology and National Chin Yi University of Technology, Taiwan, respectively. His research interests are in biomedical engineering and automation. (atclouding@yahoo.com.tw)

Kai-Jung Chen is an accomplished individual with a bachelor's degree in engineering (2010), a master's degree in biomechanical engineering (2012) from National Cheng Kung University in Taiwan, and a Ph.D. degree in engineering (2019) from the University of Liverpool, UK. From 2014 to 2019, he played a pivotal role in the Biomechanical Engineering Group at the University of Liverpool, focusing on precision ophthalmic equipment development. Since 2020, he has been a faculty member in the Department of Mechanical Engineering at National Chin- Yi University of Technology, Taiwan. His diverse research interests include computational biomechanics, medical assistive device development, big data and AI technology, and semiconductor and brittle material processing. (hskchen5@ncut.edu.tw)

Wei-Shen Kuo received his M.S. and Ph.D. degrees in mechanical engineering in 1999 and 2005 from Da-Yeh University and National Chiao Tung University, Taiwan, respectively. He was with the SPIL Research Center as a senior engineer involved in thermal management for electronic packaging. He joined the Department of Mechanical Engineering, National Chung Hsing University, Taichung, Taiwan, in January 2014, before entering the Testing Center for Technological and Vocational Education in 2022 as a research fellow. His current research interests include machine tool dynamic analysis, electronic cooling techniques, active flow control technologies, and the MEMS fabrication process. (kuows.me88g@nctu.edu.tw)